FORMATION OF BAINITE BELOW MARTENSITE START TEMPERATURE IN QUENCHING LOW CARBON STEEL

N. Yu. Zolotorevsky [1] ✉**, Yu. A. Belikova** [2]**, S. N. Petrov** [2, 1]**, A. A. Zisman** [2, 1]

[1] Peter the Great St. Petersburg Polytechnic University, St. Petersburg, Russia;

[2] NRC "Kurchatov Institute" – CRISM "Prometey", St. Petersburg, Russia

✉ zolotorevsky@phmf.spbstu.ru

Abstract. According to the phase transformation kinetics that we recorded by dilatometry in rapid cooling of low carbon steel, some amount of isothermal bainite appeared in the middle of martensitic temperature range. Presumably caused by adiabatic heating in the exothermal transformation, such an unexpected effect was confirmed by TEM data on the lath thickness, dislocation density and carbide particles. Furthermore, to assess a volume fraction of the detected bainite, statistics of crystal curvature (orientation gradient) was analyzed in terms of EBSD data. The combined analysis of results obtained using those three techniques suggests that certain amount of lath type bainite is formed not only below the martensite start temperature but also slightly above it.

Keywords: microstructure, martensite, bainite, isothermal transformation, quenching, low carbon steel

ОБРАЗОВАНИЕ БЕЙНИТА В ТЕМПЕРАТУРНОМ ИНТЕРВАЛЕ МАРТЕНСИТНОГО ПРЕВРАЩЕНИЯ ПРИ ЗАКАЛКЕ НИЗКОУГЛЕРОДИСТОЙ СТАЛИ

Н. Ю. Золоторевский [1] ✉**, Ю. А. Беликова** [2]**,
С. Н. Петров** [2, 1]**, А. А. Зисман** [2, 1]

[1] Санкт-Петербургский политехнический университет Петра Великого,
Санкт-Петербург, Россия;

[2] НИЦ «Курчатовский институт» – ЦНИИ КМ «Прометей», Санкт-Петербург, Россия

✉ zolotorevsky@phmf.spbstu.ru

Аннотация. В соответствии с кинетикой фазового превращения, зарегистрированной методом дилатометрии при быстром охлаждении низкоуглеродистой стали, в середине температурного диапазона мартенситного превращения образуется некоторое количество изотермического бейнита. Такой неожиданный эффект, предположительно вызванный

адиабатическим нагревом при неизотермическом превращении, подтверждается данными просвечивающей электронной микроскопии о толщине реек, плотности дислокаций и частицах карбидов. Кроме того, для оценки объемной доли обнаруженного бейнита на основе данных метода дифракции отраженных электронов проанализирована статистика кривизны кристаллической решетки (градиент ориентации). Совместный анализ результатов, полученных с помощью этих трех методов, позволяет заключить, что определенное количество бейнита реечного типа образуется не только ниже температуры начала мартенситного превращения, но и немного выше нее.

Ключевые слова: микроструктура, мартенсит, бейнит, изотермическое превращение, закалка, низкоуглеродистая сталь

Introduction

In order to control the proportion of martensite and bainite microstructures in high-strength steels, isothermal treatments [1 − 3] or decelerated cooling [4] inside the martensitic temperature range attract an increasing researchers' attention. In principle, with allowance for adiabatic heating due to the exothermal transformation and for numerous nucleation sites at the α-γ boundaries of preformed martensite, appearance of bainite seems possible even in case of rapid cooling. However, to the authors' knowledge, such effects have never been reported, except for Ref. [5] where dilatometry data on low carbon steel indicated a short near-isothermal stage of bainitic transformation after a notable martensite amount accumulates.

To verify this uncommon behavior, the present work analyzes the underlying microstructures by independent Transmission Electron Microscopy (TEM) and Electron Backscatter Diffraction (EBSD) methods. The former evaluates local dislocation densities and lath thickness as well as images fine carbide particles if any; the latter technique reveals the distribution of crystal curvature indicative of martensite and bainite fractions.

Material and methods

Chemical composition of the studied steel (wt. %: 0.09C, 0.35Mn, 0.30Si, 5.50[Ni+Cu], 1.50[Mo+Cr], 0.15V) ensured its mostly martensitic microstructures after quenching in a wide range of cooling rates. Start and finish temperatures of the underlying transformation slightly increase when the slower cooling and hence deviate from the athermal nature of martensite expressed by the Koinstinen − Marburger equation [6]. It remains a subject of dispute whether similar effects are due to specific (thermally activated) martensite embryos or a minor fraction of preformed lath bainite [7].

Reheated to 950°C and hold for 100 s, small specimens (Diam5×10 mm) of the steel have been quenched in DIl 805 A/D dilatometer at 60°C/s cooling rate. To confirm their somewhat unexpected response considered below in this work, such experiments were repeated several times. Following Ref. [8], to properly evaluate the transformation degree in terms of the specimen length, we allow for the temperature dependence of thermal expansion coefficients in both the parent and product phases. When neglecting this issue, the martensite start temperature would be overestimated by ~20 to 40°C.

To analyze obtained microstructures by TEM FEI Tecnai G2 30 S-TWIN at an accelerating voltage of 200 kV, disks of 1 mm thickness cut from the quenched specimen were conventionally thinned by mechanical and electrolytic polishing. Surface oxide films were then removed from prepared foils by ion milling system Fischione 1010. The lath thickness, dislocation density and morphology of carbide particles, if any, were analyzed in various microstructure constituents. Owing to the apparent width of linear defects and their mutual screening through the foil thickness, reliable estimates of the dislocation density were limited to about $6.5 \cdot 10^{10}$ cm^{-2}. Nonetheless, the revealed types of martensite and bainite can be discriminated. Since the TEM technique is essentially local, the analysis of each foil was repeated on twenty domains of 6×6 μm randomly distributed over an area of 720 μm^2. Though the eventual averaging hardly ensures true representativeness, it still enables recognition and comparison of coexisting microstructural types. Fractions of them are approximately assessed by counting related pixels of digitized images.

A planar section prepared by usual metallographic procedures and additionally subjected to electrolytic polishing has been analyzed by EBSD on SEM Lyra 3-XM at an accelerating voltage of 20 kV. An area having a width and height of 100 μm was scanned with a step of 0.05 μm, and crystal orientations at periodically arranged points were determined by means of Chanel 5 software. A subsequent analysis of the EBSD maps was carried out using MTEX software [9]. Respective levels of crystal curvature were assessed by the kernel average misorientation (KAM), that is, an average angle of lattice rotations at next neighbors of the considered data point with respect to the latter. Then a rather noisy KAM was averaged in microstructural elements separated by closed boundaries with tolerance angle $\theta_t = 4°$. The resulting "grain average" misorientation (GAM) characterizes each martensite or bainite block as a whole since the employed θ_t is a lower bound for misorientations between admitted variants of orientation relationship (OR) peculiar to shear transformations in steels [10].

Treatment of experimental data

A temperature dependence of the transformed fraction in quenching was conventionally evaluated in terms of the thermal expansions, and the considered near-isothermal origination of bainite was verified by TEM and EBSD as follows.

Recognition of microstructures by TEM. Various microstructural constituents in quenched steel have been discriminated by TEM; they are lath martensite (LM) and bainite (LB), auto-tempered martensite (AM) and granular bainite (GB). The first and second of them are ascribed to domains of near-parallel laths whose thickness does not exceed 0.8 μm; then LM is separated owing to its relatively high dislocation densities ($\rho > 6.5 \cdot 10^{10}$ cm^{-2}) and usually finer (< 0.3 μm) laths. It is kept in mind as well that bainitic domains usually contain more amounts of retained austenite.

Close dislocation densities diminished with respect to harder constituents are peculiar to both AM and GB, where domains of the former are recognizable owing to large (several microns) dimensions. Besides, this phase contains characteristic rod-like particles of cementite oriented along three crystallographic directions. Such precipitations remain thin because of relatively slow carbon diffusion at the transformation temperature.

Analysis of crystal curvature statistics. Determined by EBSD, the GAM measure of crystal curvature is due to both the dislocation density in structural elements and inhomogeneous phase stresses. Thus, there are two characteristic scales corresponding to the dislocation spacing and lath thickness. To extract each of the related contributions is problematic [11]; at the same time, their integral effect enables a rough discrimination between various constituents of the transformation product [12 − 15]. As neighboring crystals may have overlapping ranges of curvature, an analysis of its overall statistics (spectrum) rather than local data is preferable as shown in Ref. [5, 16]. Making use of this expedient, we will fit to a right tail (higher curvature range) of the experimental GAM spectrum a virtual lognormal part presumably involving martensite constituents: the LM and AM fractions. Although the latter have lower dislocation densities, its GAM keeps high according to strong phase stresses of martensite. Thus, the fraction of bainite constituents can be evaluated by subtracting the fitted spectrum from the experimental one. Relevance of this approach will be confirmed by TEM results and independent dilatometry data on the transformation kinetics.

Results and discussion

Transformation kinetics. A temperature dependence of the transformation degree F according to dilatometry data is represented in Fig. 1, a. In general, it fits perfectly with the Koinstinen − Marburger equation [6] with nucleation temperature T_{KM} of about 300°C, though above the latter a minor part of transformed phase deviates from the athermal model. Besides, a near-isothermal (presumably bainitic) segment appears at the maximum slope of this curve after a notable amount of the preformed martensite. This particular effect is supported by Fig. 1, b showing a rather smooth time dependence of the transformed fraction that excludes experimental artifacts. The most plausible explanation of the considered finding is intensive adiabatic heating due to the exothermal transformation. According to the diagram in Fig. 1, a, the portions of about 13% and 8% of the transformed matter are not due to athermal martensite [6] but contain alternative phases thermally activated, at $T > T_{KM}$ and during the above-considered stage, respectively.
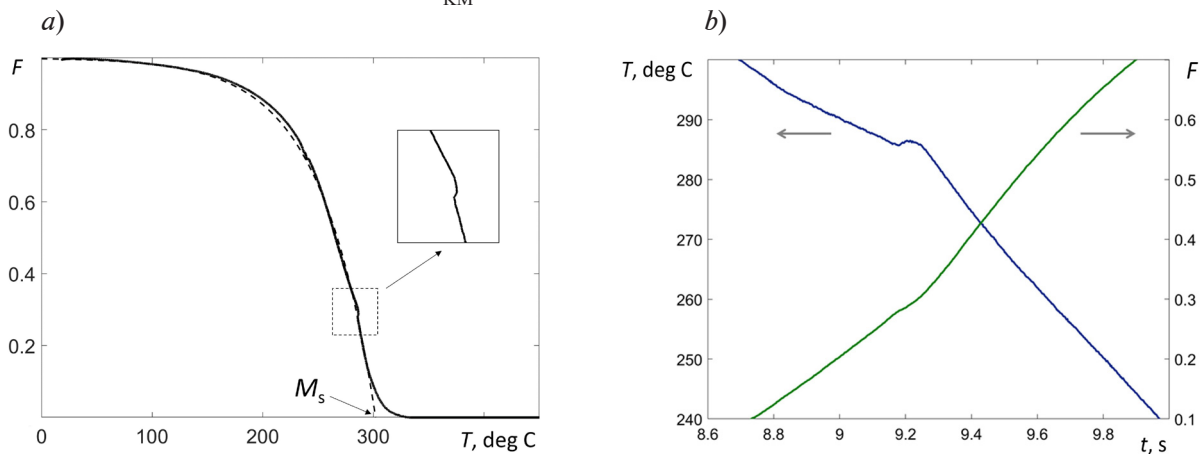

Fig. 1. Transformation kinetics in quenching low carbon martensitic steel: (a) the whole diagram where the insert indicates an isothermal stage; (b) time dependence of the temperature and the transformed fraction within the period that includes the isothermal stage.
A dashed line in (a) corresponds to the athermal transformation according to the Koinstinen − Marburger equation (see Ref. [6])

TEM data. TEM results for microstructures of LM and AM, as well as of LB and GB, are presented respectively from Fig. 2 to Fig. 5. As previously described, these results enable assessment of the considered constituent fractions. Dislocation densities in each of them were determined on several fields under identical diffraction conditions while the foil thickness was evaluated by the electron energy loss spectroscopy. Foils were oriented to get (110) planes very slightly deviated from the reflecting ("two-beam") position. Thus, high orientation gradients near dislocation cores result in dark traces of dislocation lines on the light field images with a high magnification. Besides, lower magnifications were applied to show a general appearance of transformation microstructures.

The light field image with a typical LM microstructure is represented in Fig. 2, a and the diffraction pattern in Fig. 2, b confirms a specific orientation of (110) planes. The LM occupying about 33% of the analyzed foil has thin and straight inter-lath boundaries where streaks of retained austenite and, sometimes, fine carbides are observed. The lath thickness varies from 50 to 290 nm and its average value is 160 nm. The average dislocation density of $7.0 \cdot 10^{10}$ cm^{-2} evaluated in this most hard constituent exceeds the above-mentioned limit of $6.5 \cdot 10^{10}$ cm^{-2} that would ensure accurate assessments by TEM.

Fig. 3, a−c represents corresponding TEM results for AM that is a type of martensite formed at higher temperatures. Moreover, Fig. 3, d images thin elongated particles of cementite oriented along three crystallographic directions and peculiar to this microstructure type. Its measured volume fraction equals 37% and structural units reaching 2−3 µm in width are rather large for the whole analyzed area of 720 µm^2. As expected, their evaluated dislocation density of $5.4 \cdot 10^{10}$ cm^{-2} proved to be reduced relative to that of LM.
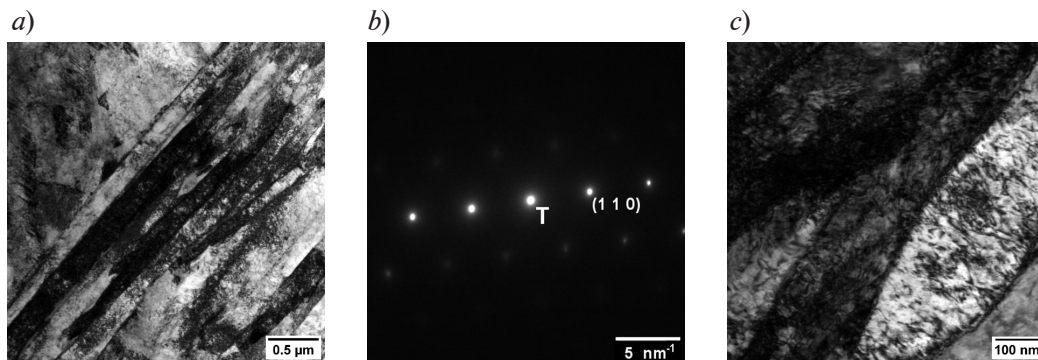
Fig. 2. TEM images of lath martensite: (*a*) general appearance by a light field image,
(*b*) a diffraction pattern at (110) planes in the reflecting orientation,
(*c*) dislocation traces imaged by dark streaks within the laths
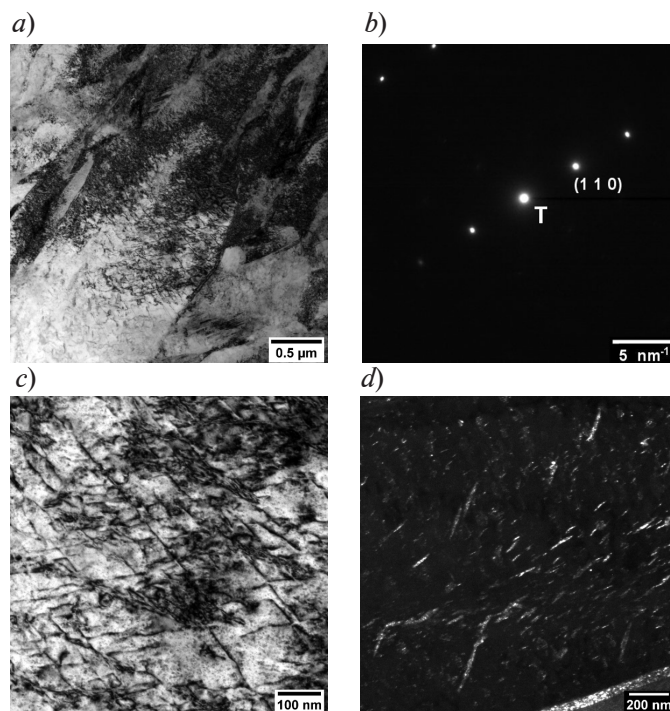

Fig. 3. TEM images of auto-tempered martensite: (*a*) general appearance by a light field image,
(*b*) a diffraction pattern at (110) planes in the reflecting orientation,
(*c*) dislocation traces imaged by dark streaks, (*d*) a dark field image of oriented carbide particles

According to the above-considered data, a martensite fraction of nominally martensitic steel quenched at very high cooling rate of 60°C/s reaches only 70% so that a notable residual fraction is presumably due LB or/and GB phases. The following TEM and EBSD results represented in Figs. 4, 5 and 6, respectively, should verify this uncommon finding and then enable evaluation of the LB-to-GB proportion.

It is very hard to recognize LB and separate the latter from LM based only on morphological signs. Indeed, the thickness of GB laths varies from 80 to 900 nm and often approach values of up to $250 - 300$ nm that is close to an upper bound for martensite laths. The average dislocation density of LB is $6.5 \cdot 10^{10}$ cm^{-2} rather close to measured $7.0 \cdot 10^{10}$ of LM though still enabling discrimination between the two microstructures. Besides, as previously mentioned, their recognition is facilitated by more perfect and straight inter-lath boundaries in LM. As to the conventional discrimination between bainite and martensite in terms of carbide distributions, this way is hardly applicable to the considered steel since its carbon content is too low. TEM results for LB are shown in Fig. 4, and the fraction of this phase is 17%.
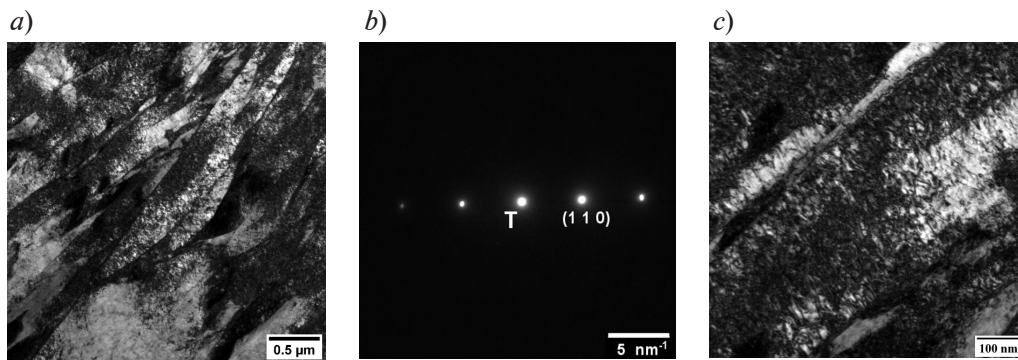
a)

b)

c)

Fig. 4. TEM images of lath bainite microstructure: (*a*) general appearance by a light field image,
(*b*) a diffraction pattern at (110) planes in the reflecting orientation,
(*c*) dislocation traces imaged by dark streaks

GB elements have sizes from 0.5 to 0.7 μm and occupy a 13% fraction of the analyzed foil area; their average dislocation density is $5.2 \cdot 10^{10}$ cm^{-2}. TEM results for this phase are shown in Fig. 5.
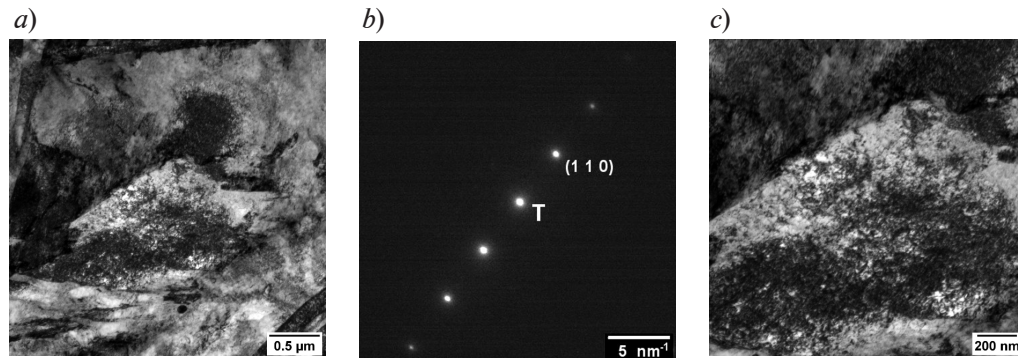
a)

b)

c)

Fig. 5. TEM images of granular bainite microstructure: (*a*) general appearance by a light field image,
(*b*) a diffraction pattern at (110) planes in the reflecting orientation,
(*c*) dislocation traces imaged by dark streaks
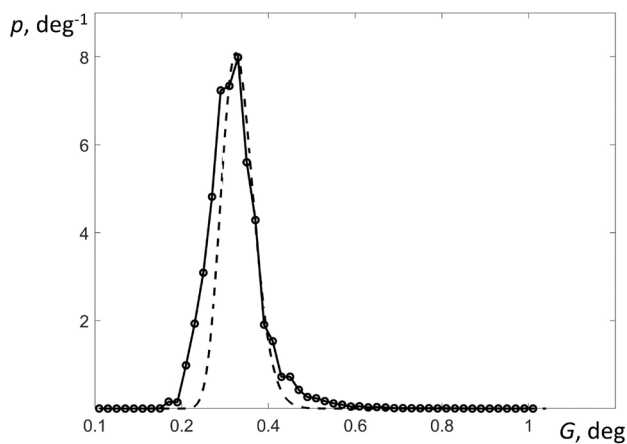
Fig. 6. A plot of probability density *p* versus crystal curvature *G* expressed by GAM function in low carbon martensitic steel quenched at the cooling rate of 60 deg C/s. A lognormal distribution is given by a dashed curve

Crystal curvature by EBSD. The fractions of steel constituents were evaluated using EBSD from the distribution of crystal curvature by a method suggested in our earlier study [5]. GAM spectrum derived by EBSD on the analyzed section is shown in Fig. 6, where a lognormal distribution (dashed curve) fitted to its right tail according to Ref. [5] corresponds to martensite constituents. To allow properly for the latter, deviations of fitted values from the lower right part of this plot are neglected, so that a remaining sum of LB and GB constituents is attributed to the spectrum part situated left from the lognormal approximation. Thus, assessed fractions of martensite (LM plus AM) and bainite (LB plus GB) equal 80% and 20%, respectively.

Combined analysis. In order to compare results provided by the three independent techniques, they are listed in Table. The martensite fraction of 79% derived from the transformation kinetics (see Fig. 1) fits 80% according to EBSD analysis much better than this could be expected. However, the TEM data, the representativeness of which is limited, should be analyzed with a special care. On the one hand, the corresponding 70% of martensite fraction could be accepted as satisfactorily close to the previous estimates of 79% and 80%. On the other hand, the difference is still notable and hence, suggests plausible corrections of the TEM results as follows. To comply with dilatometry and EBSD data, the martensite fraction should be increased by about 10% at the expense of bainite constituents. Specifically, it would be reasonable to reduce the GB rather than LB fraction as far as the former usually appears in the considered steel at much higher temperatures. As shown on the same specimens [5], this regularity agrees well with the statistics of paring of the transformation variants admitted by the inter-phase orientation relationship. In general, taking these reasons and Fig. 1 into account, both the deviation from the athermal transformation at $T > T_{KM}$ and the near-isothermal stage at $T \approx 280°C$ are mostly due to the lath type of bainite.

Table

A comparison of results obtained by independent methods

Method	Volume fraction (%) of phase constituents			
	Martensite		Bainite	
	Lath	Auto-tempered	Lath	Granular
Transmission Electron Microscopy	37	33	17	13
Dilatometry	79 in sum*		21 in sum	
Electron Backscatter Diffraction	80 in sum		20 in sum	

* An immediate result of the athermal transformation regardless of subsequent auto-tempering.

Summary

A combined analysis of dilatometry, TEM and EBSD results confirms the near-isothermal formation of lath bainite in the middle of martensitic temperature range when quenching low carbon steel. Besides, a comparison of this independent data suggests the appearance of mostly the same bainite type at temperatures slightly above T_{KM} that leads to deviations of the transformation kinetics from the athermal martensite model [6].

REFERENCES

1. **Wei Z., Hu H., Liu M., et al.,** Effect of austempering below Ms on the microstructure and wear performance of a low-carbon bainitic steel, Metals. 12 (1) (2022) 104.

2. **Qian L., Li Z., Wang T., et al.,** Roles of pre-formed martensite in below-Ms bainite formation, microstructure, strain partitioning and impact absorption energies of low-carbon bainitic steel, J. Mater. Sci. Technol. 96 (1) (2022) 69−84.

3. **Rampelberg C., Allain S. Y. P., Geandier G., et al.,** Carbide-free bainite transformations above and below martensite start temperature investigated by *in-situ* high-energy X-ray diffraction, JOM. 73 (11) (2021) 3181−3194.

4. **Zhang X., Yu H., Li Q., Song C., Yang S.,** Study of microstructural evolution and mechanical properties of 1000 MPa low-carbon micro-alloyed steel prepared by multiple quenching strategies near Ms, Mater. Sci. Eng. A. 840 (4) (2022) 142968.

5. **Zisman A. A., Zolotorevsky N. Y., Petrov S. N., Ermakova N. Y.,** Effect of cooling rate on the bainite fraction in low carbon martensitic steel: combined analysis of transformation kinetics and crystal curvature, Lett. Mater. 13 (1) (2023) 67−72.

6. **Koistinen D. P., Marburger R. E.,** A general equation prescribing the extent of austenite-martensite transformation in pure iron-carbon alloys and plain carbon steels, Acta Metall. 7 (1) (1959) 59−60.

7. **Jeyabalan K., Catteau S. D., Teixeira J., et al.,** Modeling of the austenite decomposition kinetics in a low-alloyed steel enriched in carbon and nitrogen, Materialia. 9 (March) (2020) 100582.

8. **Choi S.,** Model for estimation of transformation kinetics from the dilatation data during a cooling of hypoeutectoid steels, Mater. Sci. Eng. A. 363 (1−2) (2003) 72−80.

9. **Hielscher R., Silbermann C. B., Schmidl E., Ihlemann J.,** Denoising of crystal orientation maps, J. Appl. Cryst. 52 (5) (2019) 984−996.

10. **Takayama N., Miyamoto G., Furuhara T.,** Effect of transformation temperature on variant pairing of bainitic ferrite in low carbon steel, Acta Mater. 60 (5) (2012) 2387−2396.

11. **Zisman A.,** Choice of scalar measure for crystal curvature to image dislocation substructure in terms of discrete orientation data, J. Mech. Behav. Mater. 25 (1−2) (2016) 15−22.

12. **Wright S. I., Nowell M. M., Field D. P.,** A review of strain analysis using electron backscatter diffraction, Microsc. Microanal. 17 (3) (2011) 316−329.

13. **Gazder A. A., Al-Harbi F., Spanke H. Th., et al.,** A correlative approach to segmenting phases and ferrite morphologies in transformation-induced plasticity steel using electron back-scattering diffraction and energy dispersive X-ray spectroscopy, Ultramicroscopy. 147 (Dec) (2014) 114−132.

14. **Breumier S., Martinez Ostormujof T., Frincu B., et al.,** Leveraging EBSD data by deep learning for bainite, ferrite and martensite segmentation, Mater. Charact.186 (April) (2022) 111805.

15. **Santos D. B., Camey K., Barbosa R., et al.,** Complex phase quantification methodology using electron backscatter diffraction (EBSD) on low manganese high temperature processed (HTP) microalloyed steel, J. Mater. Res. Technol. 8 (2) (2022) 2423−2431.

16. **Zisman A. A., Petrov S. N., Zolotorevsky N. Y., Ermakova N. Y.,** Spectra of crystal curvature in terms of EBSD data to assess martensite fraction in bainitic steel, Mater. Phys. Mech. 51 (2) (2023) 227−234.

СПИСОК ЛИТЕРАТУРЫ

1. **Wei Z., Hu H., Liu M., Tian J., Xu G.** Effect of austempering below Ms on the microstructure and wear performance of a low-carbon bainitic steel // Metals. 2022. Vol. 12. No. 1. P. 104.

2. **Qian L., Li Z., Wang T., Li D., Zhang F., Meng J.** Roles of pre-formed martensite in below-Ms bainite formation, microstructure, strain partitioning and impact absorption energies of low-carbon bainitic steel // Journal of Materials Science and Technology. 2022. Vol. 96. No. 1. Pp. 69−84.

3. **Rampelberg C., Allain S. Y. P., Geandier G., Teixeria J., Lebel F., Sourmail T.** Carbide-free bainite transformations above and below martensite start temperature investigated by *in-situ* high-energy X-ray diffraction // JOM. 2021. Vol. 73. No. 11. Pp. 3181−3194.

4. **Zhang X., Yu H., Li Q., Song C., Yang S.** Study of microstructural evolution and mechanical properties of 1000 MPa low-carbon micro-alloyed steel prepared by multiple quenching strategies near Ms // Materials Science and Engineering: A. 2022. Vol. 840. 18 April. P. 142968.

5. **Zisman A. A., Zolotorevsky N. Y., Petrov S. N., Ermakova N. Y.** Effect of cooling rate on the bainite fraction in low carbon martensitic steel: combined analysis of transformation kinetics and crystal curvature // Письма о материалах. 2023. Т. 13. № 1. С. 67−72.

6. **Koistinen D. P., Marburger R. E.** A general equation prescribing the extent of austenite-martensite transformation in pure iron-carbon alloys and plain carbon steels // Acta Metallurgica. 1959. Vol. 7. No. 1. Pp. 59−60.

7. **Jeyabalan K., Catteau S. D., Teixeira J., Geandier G., Denand B., Dulcy J., Denis S., Michel G., Courteaux M.** Modeling of the austenite decomposition kinetics in a low-alloyed steel enriched in carbon and nitrogen // Materialia. 2020. Vol. 9. March. P. 100582.

8. **Choi S.** Model for estimation of transformation kinetics from the dilatation data during a cooling of hypoeutectoid steels // Materials Science and Engineering: A. 2003. Vol. 363. No.1−2. Pp. 72−80.

9. **Hielscher R., Silbermann C. B., Schmidl E., Ihlemann J.** Denoising of crystal orientation maps // Journal of Applied Crystallography. 2019. Vol. 52. Part 5. Pp. 984−996.

10. **Takayama N., Miyamoto G., Furuhara T.** Effect of transformation temperature on variant pairing of bainitic ferrite in low carbon steel // Acta Materialia. 2012. Vol. 60. No. 5. Pp. 2387−2396.

11. **Zisman A.** Choice of scalar measure for crystal curvature to image dislocation substructure in terms of discrete orientation data // Journal of the Mechanic Behavior of Materials. 2016. Vol. 25. No. 1−2. Pp. 15−22.

12. **Wright S. I., Nowell M. M., Field D. P.** A review of strain analysis using electron backscatter diffraction // Microscopy and Microanalysis. 2011. Vol. 17. No. 3. Pp. 316−329.

13. **Gazder A. A., Al-Harbi F., Spanke H. Th., Mitchel D. R. G., Pereloma E. V.** A correlative approach to segmenting phases and ferrite morphologies in transformation-induced plasticity steel using electron back-scattering diffraction and energy dispersive X-ray spectroscopy // Ultramicroscopy. 2014. Vol. 147. December. Pp. 114−132.

14. **Breumier S., Martinez Ostormujof T., Frincu B., Gey N., Couturier A., Loukachenko N., Abaperea P. E., Germain L.** Leveraging EBSD data by deep learning for bainite, ferrite and martensite segmentation // Materials Characterization. 2022. Vol. 186. April. P. 111805.

15. **Santos D. B., Camey K., Barbosa R., Andrade M. S., Escobar D. P.** Complex phase quantification methodology using electron backscatter diffraction (EBSD) on low manganese high temperature processed (HTP) microalloyed steel // Journal of Materials Research and Technology. 2022. Vol. 8. No. 2. Pp. 2423−2431.

16. **Zisman A. A., Petrov S. N., Zolotorevsky N. Y., Ermakova N. Y.,** Spectra of crystal curvature in terms of EBSD data to assess martensite fraction in bainitic steel // Materials Physics and Mechanics. 2023. Vol. 51. No. 2. Pp. 50−57.

THE AUTHORS

ZOLOTOREVSKY Nikolay Yu.
Peter the Great St. Petersburg Polytechnic University
29 Politechnicheskaya St., St. Petersburg, 195251, Russia
zolotorevsky@phmf.spbstu.ru
ORCID: 0000-0002-0185-5452

BELIKOVA Yulia A.
NRC "Kurchatov Institute" − CRISM "Prometey"
49 Shpalernaya St., St. Petersburg, 191015, Russia
belikjul@ya.ru

PETROV Sergey N.
NRC "Kurchatov Institute" − CRISM "Prometey"
Peter the Great St. Petersburg Polytechnic University
49 Shpalernaya St., St. Petersburg, 191015, Russia
petrov.epma@mail.ru
ORCID: 0000-0001-6732-7217

ZISMAN Alexander A.
NRC "Kurchatov Institute" − CRISM "Prometey"
Peter the Great St. Petersburg Polytechnic University
49 Shpalernaya St., St. Petersburg, 191015, Russia
crism_ru@yahoo.co.uk
ORCID: 0000-0002-9431-7097

СВЕДЕНИЯ ОБ АВТОРАХ

ЗОЛОТОРЕВСКИЙ Николай Юльевич − *доктор физико-математических наук, профессор Высшей школы механики и процессов управления Санкт-Петербургского политехнического университета Петра Великого, Санкт-Петербург, Россия.*
195251, Россия, г. Санкт-Петербург, Политехническая ул., 29
zolotorevsky@phmf.spbstu.ru
ORCID: 0000-0002-0185-5452

БЕЛИКОВА Юлия Александровна — *научный сотрудник ФГУП "Центральный научно-исследовательский институт конструкционных материалов «Прометей» имени И. В. Горынина" Национального исследовательского центра «Курчатовский институт», Санкт-Петербург, Россия.*

191015, Россия, г. Санкт-Петербург, Шпалерная ул., 49

belikjul@ya.ru

ПЕТРОВ Сергей Николаевич — *доктор технических наук, кандидат химических наук, старший научный сотрудник ФГУП "Центральный научно-исследовательский институт конструкционных материалов «Прометей» имени И. В. Горынина" Национального исследовательского центра «Курчатовский институт», профессор базовой кафедры «Функциональные материалы и технологии» Санкт-Петербургского политехнического университета Петра Великого, Санкт-Петербург, Россия.*

191015, Россия, г. Санкт-Петербург, Шпалерная ул., 49

petrov.epma@mail.ru

ORCID: 0000-0001-6732-7217

ЗИСМАН Александр Абрамович — *доктор физико-математических наук, главный научный сотрудник ФГУП "Центральный научно-исследовательский институт конструкционных материалов «Прометей» имени И. В. Горынина" Национального исследовательского центра «Курчатовский институт», профессор Высшей школы механики и процессов управления Санкт-Петербургского политехнического университета Петра Великого, Санкт-Петербург, Россия.*

191015, Россия, г. Санкт-Петербург, Шпалерная ул., 49

crism_ru@yahoo.co.uk

ORCID: 0000-0002-9431-7097